BMC Microbiology

RESEARCH

Open Access

Antivirulence activities of Rutin-loaded chitosan nanoparticles against pathogenic *Staphylococcus aureus*

Fatemeh Esnaashari[1] and Hossein Zahmatkesh[2*]

Abstract

Background *Staphylococcus aureus* is an infectious bacterium that is frequently found in healthcare settings and the community. This study aimed to prepare rutin-loaded chitosan nanoparticles (Rut-CS NPs) and assess their antibacterial activity against pathogenic strains of *S. aureus*.

Results The synthesized Rut-CS NPs exhibited an amorphous morphology with a size ranging from 160 to 240 nm and a zeta potential of 37.3 mV. Rut-CS NPs demonstrated significant antibacterial activity against *S. aureus* strains. Following exposure to Rut-CS NPs, the production of staphyloxanthin pigment decreased by 43.31–89.63%, leading to increased susceptibility of *S. aureus* to hydrogen peroxide. Additionally, visual inspection of cell morphology indicated changes in membrane integrity and permeability upon Rut-CS NPs exposure, leading to a substantial increase (107.07–191.08%) in cytoplasmic DNA leakage in the strains. Furthermore, ½ MIC of Rut-CS NPs effectively inhibited the biofilm formation (22.5–37.5%) and hemolytic activity (69–82.59%) in the *S. aureus* strains.

Conclusions Our study showcases that Rut-CS NPs can serve as a novel treatment agent to combat *S. aureus* infections by altering cell morphology and inhibiting virulence factors of *S. aureus*.

Keywords Rut-CS NPs, Staphyloxanthin, Cytoplasmic leakage, Membrane integrity, Biofilm

Background

Staphylococcus aureus is a Gram-positive opportunistic pathogen that is responsible for diverse infections in both healthcare settings and the community. This bacterium is implicated in a broad spectrum of diseases, including endocarditis, osteomyelitis, soft tissue, and urinary tract infections. Furthermore, *S. aureus* expresses a multitude of potential virulence factors, such as hemolysins, exotoxins, lipase, and coagulase which facilitate tissue invasion and infection development [1, 2].

While there are numerous antibacterial medications in the pharmaceutical market, ongoing research on potent antimicrobial agents is crucial, especially those with novel mechanisms. This is essential to prevent the rise of resistance against existing antibacterial agents and to provide effective treatment options for antibiotics-resistant infections [3]. Traditional medicine has historically relied on the use of medicinal plants. Presently, natural compounds like curcumin, quercetin, and rutin (Rut) have garnered attention for their cost-effectiveness, safety profile, and therapeutic efficacy [4].

Rut is a greenish-yellow powder belonging to the flavonol class, and was first identified in 1842. According

*Correspondence:
Hossein Zahmatkesh
h.zahmatkesh@iau.ir
[1]Department of Biology, Lahijan Branch, Islamic Azad University, Lahijan, Iran
[2]Department of Microbiology, Lahijan Branch, Islamic Azad University, Lahijan, Iran

to reports, Rut is present in over 70 species of plants, so that grapes and buckwheat are known to have the highest concentrations of Rut compared to other plant species. The manifold health benefits of Rut for humans have been recognized, including its antioxidant, anti-inflammatory, and anticancer properties. Additionally, Rut has exhibited antibacterial activity against various bacterial strains, including *Pseudomonas aeruginosa*, *S. aureus*, and *Escherichia coli* [5].

Rut has the ability to inhibit the prooxidant activities of some flavonoids. Another advantage of Rut that distinguishes it from some flavonoids such as apigenin and luteolin is its absence of cytotoxicity towards normal human cells. Hence, the non-toxic and non-oxidizing characteristics of Rut make it an exceptionally effective molecule [5]. However, the main drawback of Rut is its limited solubility in aqueous media, leading to low bioavailability [6]. Low bioavailability is a common challenge observed in various natural products, including luteolin [7] and apigenin [8]. To address this issue, polymeric and lipid nanoparticles have been extensively studied as nano-formulations to improve the bioavailability of flavonoids [5].

Chitosan (CS) is a cationic linear heteropolysaccharide of natural origin, composed of glucosamine (GlcN) and N-acetylglucosamine (GlcNAc) subunits linked through β-(1–4) glycosidic linkages. It is obtained by deacetylating chitin, the second most abundant polymer in nature. Typically, CS is sourced from crustacean shells (such as shrimp, crabs, and lobster), insect exoskeletons, and fungal cell walls. Unique characteristics of CS including biodegradability, biocompatibility, nontoxicity, and low immunogenicity lead to its widespread application in various fields such as drug delivery, biotechnology, and the food industry. Moreover, CS exhibits notable antibacterial activity against a broad spectrum of pathogens, encompassing both Gram-positive and Gram-negative bacteria [9, 10]. Furthermore, mucoadhesive properties and the ability to open cell-to-cell tight junctions of CS NPs allow them to bind to mucous membranes and gradually release the encapsulated medication through nasal, oral, pulmonary, and vaginal routes. These advantageous attributes make CS an appealing choice for encapsulating antimicrobial agents and developing innovative nanotherapeutics for combating microbial infections [11].

In previous studies, researchers have successfully encapsulated various polyphenols with antibacterial properties, such as curcumin and quercetin, using CS nanoparticles [12–14]. Nevertheless, the impact of rutin-loaded CS nanoparticles (Rut-CS NPs) on *S. aureus* has not been explored to date. Therefore, in this study, we synthesized Rut-CS NPs and investigated their antibacterial and antibiofilm properties against *S. aureus* strains.

Methods

Chemicals

Medium molecular weight chitosan (448877, 75–85% deacetylated) and rutin hydrate (R5143, purity ≥ 94.0% HPLC) were purchased from Sigma-Aldrich. Pentasodium triphosphate (TPP, 106999), and glutaraldehyde (354400, purity ≥ 98.0% TLC) were obtained from Merck. All chemicals of analytical grade were commercially available.

Preparation of Rut-CS NPs

The preparation of Rut-CS NPs was carried out using the ionic gelation technique with slight modifications [15]. Concisely, CS powder (0.1%, w/v) was dissolved in an acetic acid solution (1% v/v) under magnetic stirring at room temperature (RT) for 24 h. Subsequently, Rut solution in Dimethyl sulfoxide (DMSO) was added to the resulting transparent chitosan solution (with a final concentration of 4 mg/mL), and the pH was adjusted to 5 using sodium hydroxide (2 M). Then, TPP solution (0.1%, w/v) was prepared by dissolving it in deionized water and added dropwise into the CS-Rut solution at the 1:3 (v/v) ratio under continual stirring at 700 rpm. Following 2 h stirring, the resulting milky colloidal suspension was centrifuged at 5000 g for 20 min at 4 ˚C. The supernatant was discarded, and the pellet was washed with deionized water to eliminate unbound Rut. The pellet was dispersed in deionized water and frozen at −40 ˚C overnight. Subsequently, Rut-CS NPs were lyophilized using a freeze drier (TOPT-10 C, Toption Instrument Co., China) at -80 ˚C under 0.8 bar pressure for 72 h. The lyophilized NPs were stored at 4 ˚C for further analysis.

Characterization of Rut-CS NPs

Fourier transform infrared spectroscopy (FTIR)

The samples underwent FTIR analysis using a Thermo Nicolet Avatar 360 instrument (USA) to identify their functional groups. To achieve this, the samples were mixed with potassium bromide (KBr) and subjected to a vacuum to remove air. The powdered samples were then compressed into pellets using a press, and the pellet's spectrum was recorded in the wavelength range of 500–4000 cm^{-1} at a temperature of 25–35 °C.

X-ray diffraction (XRD)

The crystalline structure of the samples was determined through XRD analysis using a Philips PW 1730 X-ray diffractometer (Netherlands) with Cu Kα radiation (λ = 1.540598 Å). The analysis was carried out at a current of 30 mA and a voltage of 30 kV, covering diffraction angles (2θ) from 0 to 80° with a scanning step of 0.05°.

Zeta potential

The surface charge of the Rut-CS NPs was determined utilizing SZ-100z (Horiba Jobin Yvon, Japan). In brief, the particles were suspended in 50% glycerol and sonicated. The suspension was then transferred to a zeta-potential cell, and measurements were carried out at a 3.4 electrode voltage.

Dynamic light scattering (DLS)

DLS analysis was performed to assess the size distribution of the Rut-CS NPs. Initially, the Rut-CS NPs were dispersed in water, and a small volume of this suspension was loaded into the cuvette of the SZ-100z Zeta potential analyzer from Horiba Jobin Yvon. The measurements were performed at a scattering angle of 90° and RT.

Scanning electron microscopy (SEM)

The size and morphology of the Rut-CS NPs were examined using SEM analysis. The Rut-CS NPs were suspended in ethanol through sonication. Afterward, the particles were mounted on a carbon tab and coated with a thin layer of gold. Subsequently, SEM imaging was conducted using an MIRA3 TESCAN microscope (Czech Republic), operating at a voltage of 15 kV. Additionally, ImageJ software was employed for the analysis of SEM images.

Transmission electron microscopy (TEM)

TEM characterization was conducted to obtain the size and morphology of the Rut-CS NPs. The synthesized NPs were dispersed in ethanol through sonication. Then, 20 µL of the suspension was pipetted onto a copper-coated grid and dried in a vacuum chamber. Subsequently, images were acquired at 100 kV using a TEM instrument (Philips EM208S, Netherlands).

Ultra-violet visible spectroscopy (UV-Vis)

The UV–vis spectroscopy analysis of the CS and Rut-CS NPs was performed using a Unico spectrophotometer (UV-vis 2100, United States). The samples were suspended in 1 mL of DMSO, and UV-vis spectra were recorded within the wavelength range of 200 to 600 nm.

S. aureus strains

The pathogenic strains of *S. aureus* (SA01-SA05) were kindly provided by Dr. Zamani of the University of Guilan. In addition, the *S. aureus* ATCC 25923 was used as a standard strain.

Well diffusion method

The antibacterial activity of Rut-CS NPs against *S. aureus* was assessed using a well diffusion assay [16]. For this purpose, *S. aureus* with a 0.5 McFarland turbidity was cultured on the surface of Muller Hinton Agar (MHA) medium using a sterile cotton swab. Then, 6 mm diameter wells were punched on the medium, and 50 µL of different concentrations of CS, Rut, and Rut-CS NPs (10, 20, 30 mg/mL) were added to each well. The plates were then incubated at 37 ˚C for 24 h, and the diameter of the growth inhibition zone around the wells was measured in millimeters.

Determination of minimum inhibitory concentration (MIC) and minimum bactericidal concentration (MBC)

The MIC of Rut-CS NPs against *S. aureus* strains was determined using the broth micro-dilution technique as previously described [17]. Initially, various concentrations of Rut-CS NPs (ranging from 250 to 8000 µg/mL) were dispensed in a 96-well microtiter plate. Next, the bacterial suspension of the *S. aureus* strains was prepared to achieve a 0.5 McFarland density by inoculating colonies from overnight cultures in the Muller Hinton Broth (MHB) medium. The microbial suspension was then diluted in MHB at a ratio of 1:100 to the bacterial population reached 1.5×10^6 CFU/mL, and 100 µL of the diluted suspension was added to each well. The microtiter plates were kept in a 37 ˚C incubator for 24 h and then examined for bacterial growth. The lowest concentration of Rut-CS NPs that inhibited bacterial growth was considered the MIC value.

In addition, MBC was determined by inoculating 100µL from the wells with absent bacterial growth on MHA plates. Following 24 h of incubation at 37 ˚C, bacterial growth was monitored, and the lowest concentration of Rut-CS NPs that resulted in no bacterial growth was considered the MBC value.

Biofilm formation assay

The effect of Rut-CS NPs on biofilm formation in *S. aureus* strains was assessed using the crystal violet staining assay [18]. Initially, bacterial cells were cultured in 96-well plates in the presence of ½ and ¼ MIC of Rut-CS NPs. Following a 48 h incubation period, the medium containing non-adherent cells was aspirated, and the plate was washed thrice with distilled water. Next, the wells were left to air-dry, and 0.1% crystal violet solution was added to each well and allowed to incubate for 30 min at RT. Afterward, the excess dye was discarded, and the plate was washed with distilled water. To solubilize the dye, 30% acetic acid was added, and the optical density at 570 nm was measured to determine the level of biofilm formation. The wells without bacterial cells and untreated cells were considered negative and positive controls, respectively.

Staphyloxanthin inhibition assay

The inhibitory potential of the Rut-CS NPs against staphyloxanthin pigment was evaluated as previously

described [19]. Briefly, *S. aureus* strains were cultured in Tryptic Soy Broth (TSB) with (½ and ¼ MIC) or without Rut-CS NPs at 37 ˚C for 24 h. Following incubation, bacterial cells were collected through centrifugation at 4 ˚C and washed twice with distilled water. The collected pellets were subsequently resuspended in 2 mL of 99% methanol and agitated for 30 min at 55 ˚C in the dark. Afterward, the samples were centrifuged, and the absorbance of the supernatant was recorded at 465 nm using a spectrofluorometer.

Hydrogen peroxide (H_2O_2) sensitivity assay

For evaluation of H_2O_2 sensitivity, bacterial strains were inoculated in TSB without or with (½ and ¼ MIC) of Rut-CS NPs. After 24 h of incubation at 37 ˚C, the overnight cultures were swabbed on the MHA surface. Then, blank paper discs with 6 mm diameter were soaked by 30µL of H_2O_2 10% (v/v) and placed on MHA Petri dishes. Following 24 h of incubation at 37 ˚C, the diameter of the growth inhibition area was measured [20].

Analysis of cell morphology of bacterial cells treated by Rut-CS NPs

The morphological change of bacterial cells after treatment with NPs was examined by SEM as described previously [21]. Concisely, bacterial cells (1.5×10^8 CFU/mL) in the presence of ½ MIC of NPs were incubated at 37 ˚C for 16 h. Next, 10 µL of the nanoparticle-treated bacterial cells were placed on glass coverslips and air-dried. Then, bacterial cells were fixed using glutaraldehyde (2.5% v/v in PBS) at 4 ˚C for 18 h. Fixed bacterial cells were dehydrated using various concentrations of ethanol, including 20, 30, 40, 50, 60, 70, 80, and 95% for 15 min each. Eventually, coverslips were dried at RT, and cell morphology was examined by SEM using the MIRA3 TESCAN microscope (Czech Republic).

Cytoplasm leakage

To examine the impact of Rut-CS NPs on cell membrane integrity, the quantity of leaked cytoplasmic nucleic acids was measured at 260 nm. In brief, bacterial cells were inoculated into TSB with (½ and ¼ MIC) or without Rut-CS NPs and incubated at 37 ˚C for 16 h. Next, the bacterial suspension was centrifuged at 6000 rpm for 10 min, and the supernatants were collected. The DNA concentration was calculated using an EzDrop 1000 Spectrophotometer [22].

Hemolysis assay

The effect of Rut-CS NPs on the hemolytic activity of *S. aureus* isolates was assessed using the following method [23]: Bacterial cells were grown in TSB with ¼ and ½ MIC or without Rut-CS NPs for 16 h at 37 °C. After that, the bacterial culture was centrifuged at 4 °C, and the cell-free supernatant was collected for the hemolysis assay. Defibrinated sheep blood (Bahar Afshan, Iran) was centrifuged at 3000 rpm and 4 °C. The supernatant was discarded, and washed red blood cells (RBCs) were obtained after three washes with phosphate buffer saline (PBS). Washed RBCs were diluted in PBS to create a 3% RBC solution. Subsequently, 1 mL of bacterial supernatant was added to 5 mL of 3% RBC solution. This mixture was incubated in a shaker incubator at 37 °C for 1 h. Then, the suspension was centrifuged, and the absorbance of the supernatant was measured at 430 nm. Normal saline and distilled water were used as the negative and positive controls, respectively. The hemolysis inhibition rate was determined using the following equation:

Hemolysis inhibition (%) = [(Untreated OD – Treated OD)/Untreated OD] × 100.

Statistical analysis

Experiments were performed in triplicates, and the results were reported as mean±SD. Differences between the control and treatment groups were assessed by one-way analysis of variance (ANOVA) using GraphPad Prism 9 software. p-values below 0.05 were considered significant.

Results

Characterization of RUT-CS NPs

FTIR analysis

The FTIR spectra of CS (Fig. 1A) revealed characteristic peaks, including the symmetric C-H stretching at 2921 cm^{-1} and the asymmetric C-H stretching at 2879 cm^{-1}. The C=O stretching of amide I bonds was observed at 1666 cm^{-1}, while the peak at 1578 cm^{-1} indicated C=O stretching vibrations (amide 1). The C-O stretching vibrations were shown at 1156 cm^{-1} and 1076 cm^{-1}. The bands at 1439 cm^{-1} and 1377 cm^{-1} were assigned to CH_2 bending and CH_3 symmetrical deformations, respectively. The presence of the C-N stretching of amide III was confirmed by the band observed around 1322 cm^{-1}. Additionally, the peak at 896 cm^{-1} indicated the presence of monosaccharides. In the FT-IR spectra of Rut (Fig. 1B), the peak at 3441 cm^{-1} is characteristic of O-H stretching, while the peak at 2941 cm^{-1} indicates the C-H stretching vibration. Absorption bands at 1653 cm^{-1}, 1599 cm^{-1}, and 1504 cm^{-1} assigned to C=O group. The absorption peaks at 1064 cm^{-1} and 1014 cm^{-1} are characteristic of C=C stretching, and the =C-H group was illustrated at 807 cm^{-1} and 596 cm^{-1}. In the FT-IR spectra of Rut-CS NPs (Fig. 1C), the absorption bands at 1653 cm^{-1} and 1599 cm^{-1}, assigned to C-OH stretching vibration, shifted to 1651 cm^{-1} and 1575 cm^{-1}, respectively. Additionally, the absorption peak at 807 cm^{-1}, corresponding to the =C–H group, shifted to a lower wavenumber of 805 cm^{-1}. The

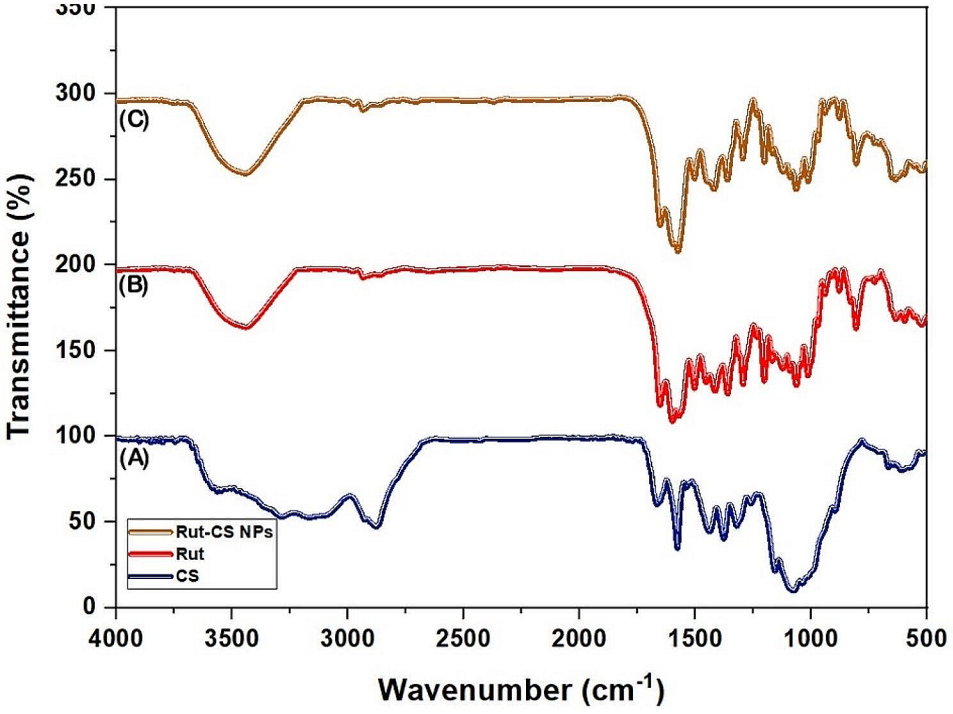

Fig. 1 Fourier Transform Infrared Spectroscopy of (**A**) Chitosan, (**B**) Rutin, and (**C**) Rutin-loaded chitosan nanoparticles

reduction in the intensity of these bands indicated the binding of Rut to CS.

XRD analysis

The XRD pattern of CS demonstrated two prominent peaks at 2θ = 11.6° and 2θ = 20.09°, indicating the presence of a crystalline structure in CS (Fig. 2A). Similarly, the XRD pattern of Rut (Fig. 2B) displayed narrow peaks at 2θ = 14.67°, 16.9°, 20.59°, 22.27°, and 26.7°, indicating the crystalline nature of Rut. The XRD examination of the Rut-CS NPs (Fig. 2C) validated the preservation of rutin's crystalline structure even following its encapsulation. However, in comparison to pure Rut, the strength of the peaks in the Rut-CS NPs was reduced. This occurrence might be due to the interaction between Rut and the CS matrix.

Zeta potential and particle size distribution

The Zeta potential value (Fig. 3A) and hydrodynamic radius (Fig. 3B) of Rut-CS NPs were 37.3 mV and 274.7 nm, respectively.

Scanning electron microscopy

SEM analysis was employed to examine the size and morphology of the synthesized Rut-CS NPs. The SEM images (Fig. 4) revealed that the NPs exhibited an amorphous structure with an average diameter of 218.5 nm.

Transmission electron microscopy

Confirmation of Rut encapsulation within CS was achieved using TEM analysis. As depicted in the results (Fig. 5), Rut, with a diameter varying from 9 to 48 nm, was effectively confined within CS nanoparticles. The size range of the Rut-CS NPs was determined to range from 160 to 240 nm.

UV-vis spectroscopy

The optical absorption of CS and Rut-CS NPs was evaluated using UV-vis spectroscopy. Based on our results, the UV-vis spectrum of CS exhibited a wide absorption band with moderate intensity at a wavelength of 300 nm. For Rut-CS NPs, a significantly higher intensity level was observed compared to the CS biopolymer. This increased intensity is attributed to the formation of nanoparticles (Fig. 6).

Well Diffusion Method

The agar well diffusion test was used to assess the antibacterial efficacy of Rut-CS NPs against different strains of *S. aureus*. The results revealed potent inhibitory effects of Rut-CS NPs, while CS and Rut alone did not produce any inhibition zones. Rut-CS NPs created a growth inhibition zone ranging from 6 to 12 mm. The visible clear zone formed by Rut-CS NPs against *S. aureus* strains is illustrated in Fig. 7A and B. Additionally, the diameters of the inhibition zones surrounding the wells are presented in Fig. 7C; Table 1.

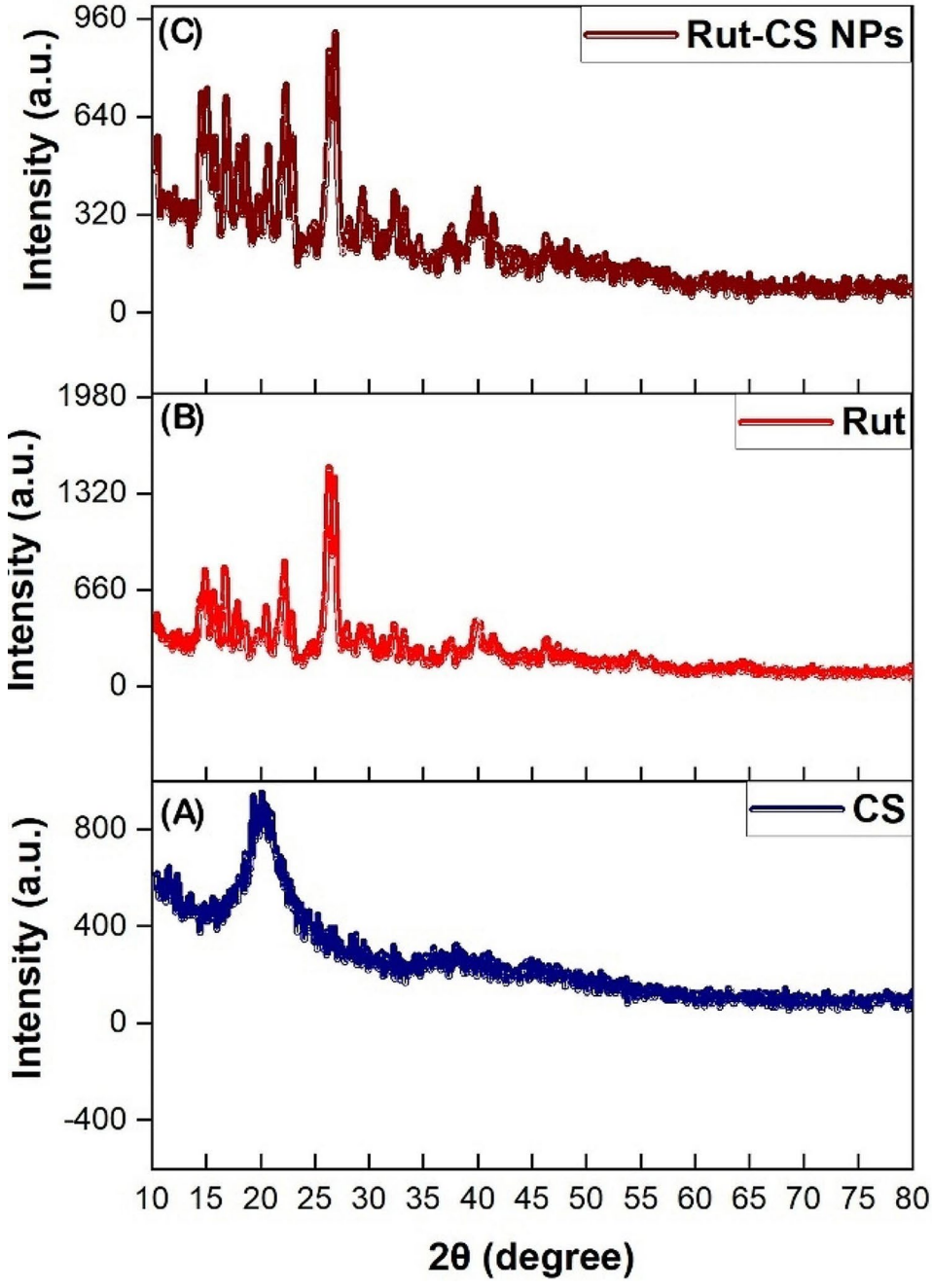

Fig. 2 X-ray diffraction pattern of (**A**) Chitosan, (**B**) Rutin, and (**C**) Rutin-loaded chitosan nanoparticles

MIC and MBC

The microdilution method was used to determine the inhibitory effect of Rut-CS NPs on *S. aureus* strains. The MIC values of Rut-CS NPs for the SA01, SA02, SA03, and SA05 strains were recorded at 1000 µg/mL. Further, the NPs inhibited the growth of SA04 and ATCC strains at a concentration of 500 µg/mL. Additionally, Rut-CS NPs had bactericidal activity against the ATCC strain at a concentration of 2000 µg/mL, whereas the NPs had no killing activity for the remaining strains.

Biofilm formation assay

The inhibitory effect of Rut-CS NPs on biofilm formation in various strains of *S. aureus* was evaluated using a Crystal violet staining assay. The results demonstrated significant inhibition of biofilm formation in most strains upon treatment with ½ MIC of NPs, with inhibition rates ranging from 22.5 to 37.5%. However, strain SA04 displayed a negligible decrease in biofilm formation. Moreover, biofilm inhibition rates of *S. aureus* strains following treatment with ¼ MIC of NPs ranged from 5.5 to 28%. The

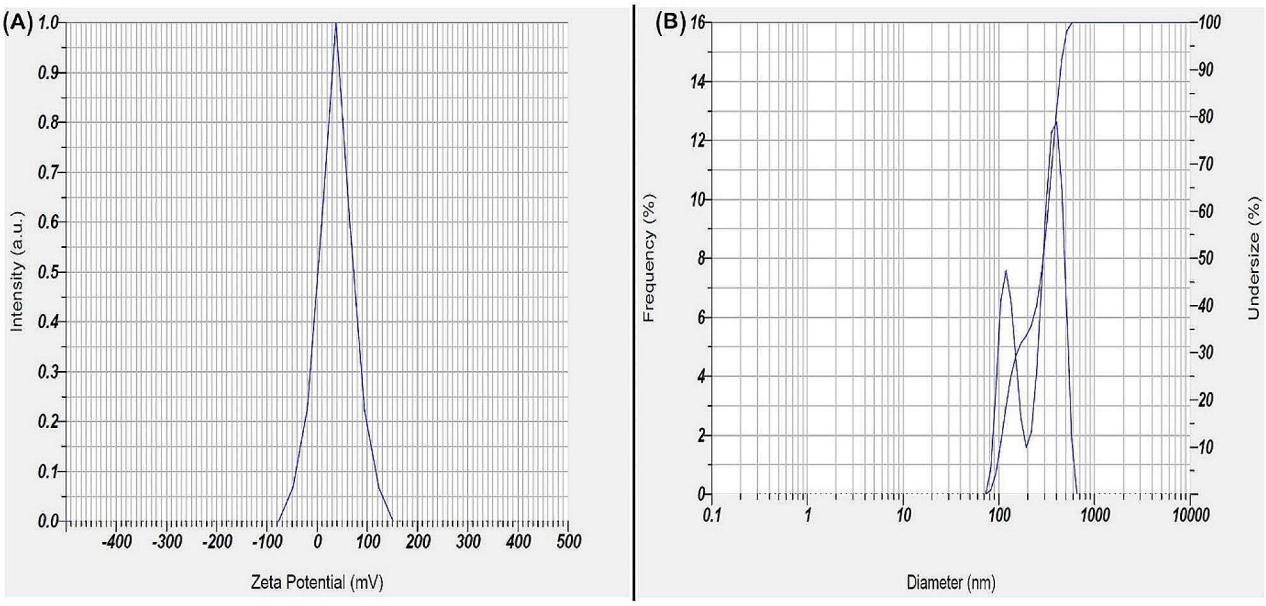

Fig. 3 (**A**) Zeta potential, and (**B**) Dynamic light scattering analysis of Rutin-loaded chitosan nanoparticles

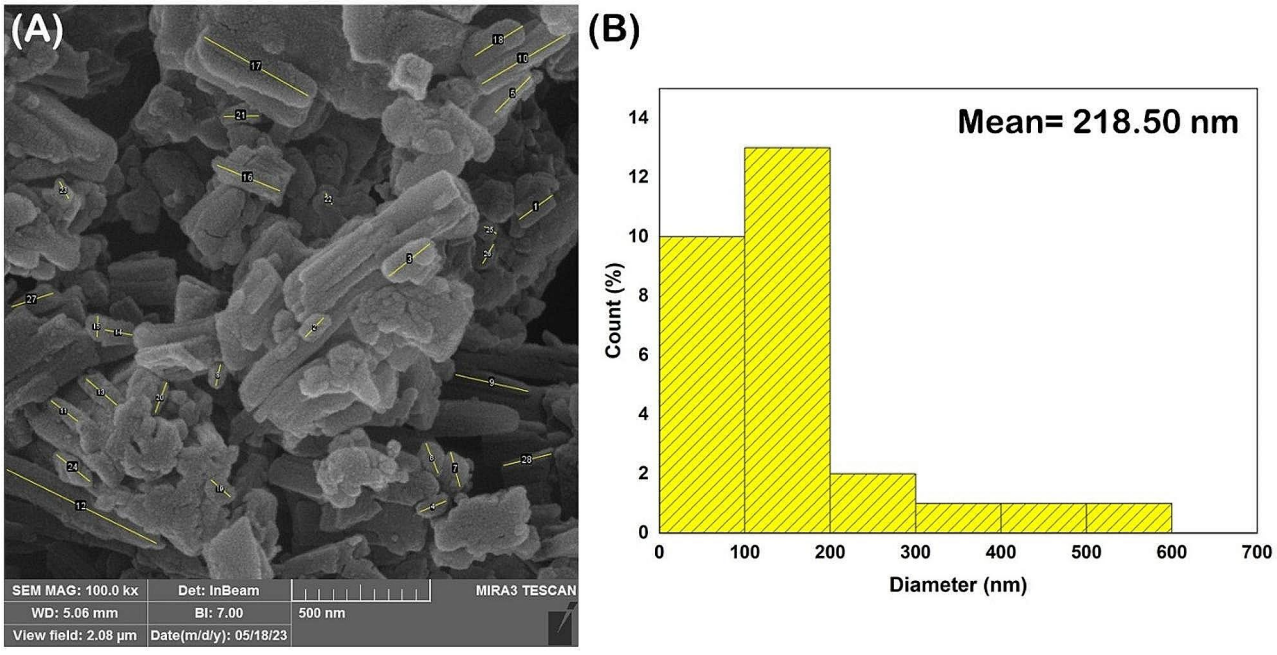

Fig. 4 (**A**) Scanning Electron Microscopy image, and (**B**) particle size distribution of Rutin-loaded chitosan nanoparticles

levels of biofilm formation by various *S. aureus* strains in the presence of Rut-CS NPs are illustrated in Fig. 8.

Staphyloxanthin inhibition assay

The ability of Rut-CS NPs to inhibit the production of staphyloxanthin pigment in *S. aureus* strains was assessed. As shown in Fig. 9, RUT-CS NPs significantly reduced the production of staphyloxanthin pigment compared to the control group. Staphyloxanthin inhibition of the ATCC strain at ¼ and ½ MIC was recorded 46% and 87%, respectively. The inhibition of staphyloxanthin for SA01-SA05 strains at ¼ MIC was recorded as 43.31%, 55.37%, 50.81%, 51.82%, and 60.22%, respectively. Meanwhile, ½ MIC resulted in an 88.48%, 87.09%, 85.79%, 89.63%, and 89.20% inhibition rate in SA01-SA05 strains, respectively.

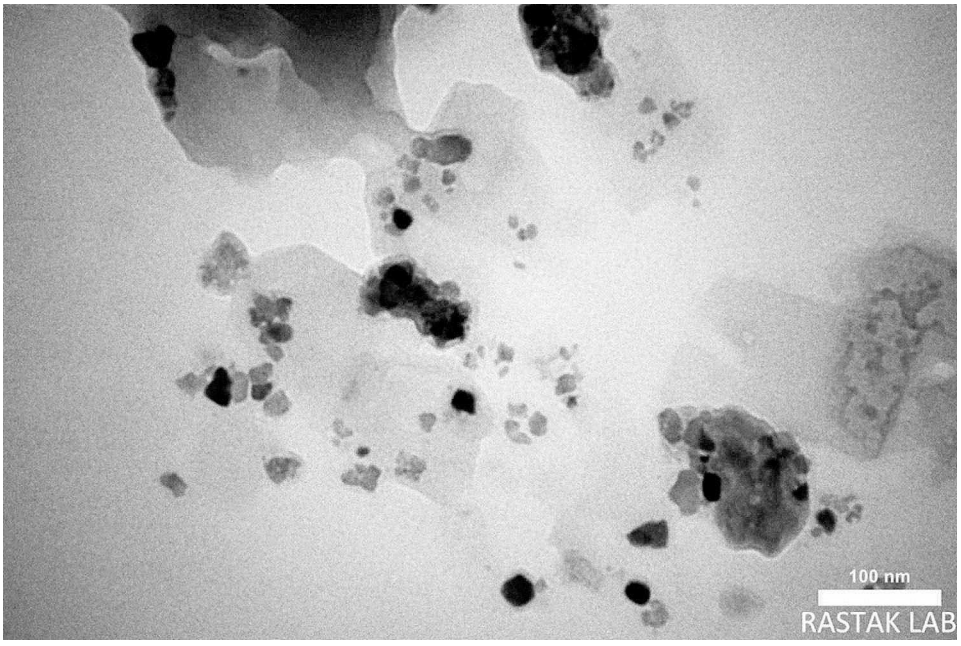

Fig. 5 Transmission electron microscopy image Rutin-loaded chitosan nanoparticles

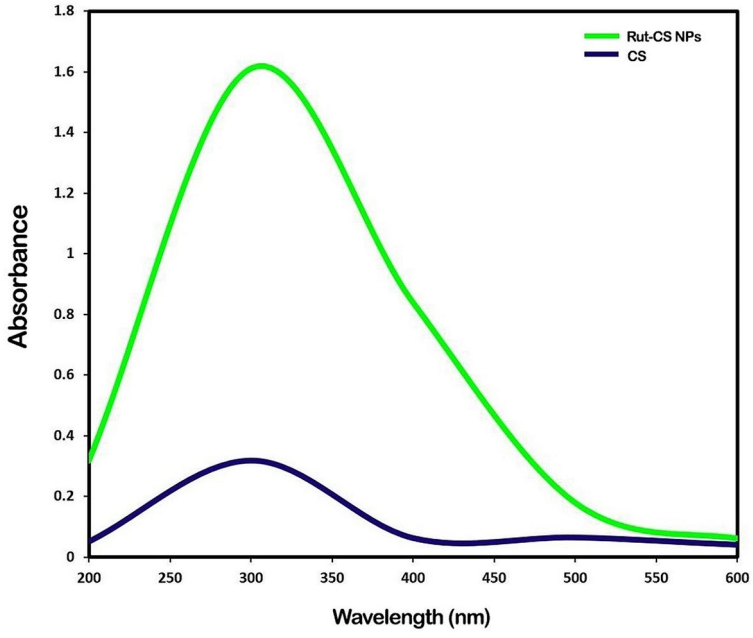

Fig. 6 Ultra-violet visible spectroscopy of Chitosan and Rutin-loaded chitosan nanoparticles

H_2O_2 sensitivity assay

Treating *S. aureus* strains with Rut-CS NPs increased the diameter of the clear halo surrounding the H_2O_2 disks. This indicates that the treatment groups of *S. aureus* were less tolerant to oxidative stress compared to the control group (Fig. 10). In SA01-SA05 strains, halos of 29.75 mm, 26.75 mm, 27.25 mm, 30.25 mm, and 30.5 mm were observed around the disks after treatment with ¼ MIC of NPs, respectively, compared to the control groups, which exhibited halos ranging from 20.5 mm to 25.75 mm. In SA01-SA05 strains, halos measuring 43.5 mm, 37.25 mm, 33.75 mm, 39 mm, and 37 mm were detected around the disks following treatment with ½ MIC of NPs, respectively. Additionally, halos of 35 mm at ¼ MIC and 44 mm at ½ MIC were observed in the ATCC strain, compared to the control group with a halo size of 24 mm.

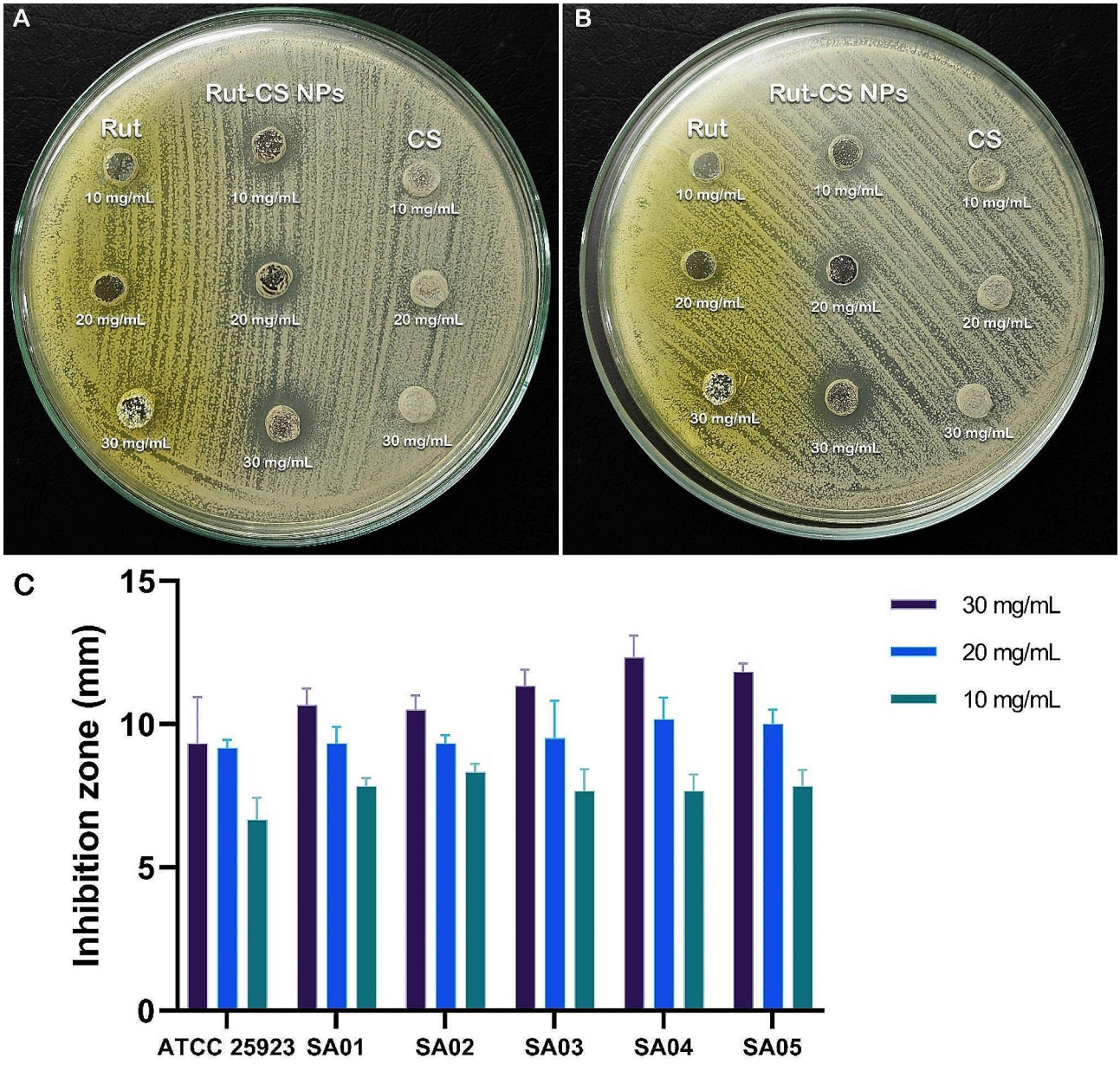

Fig. 7 Antibacterial activity of different concentrations (10, 20, and 30 mg/mL) of Rutin, Chitosan, and Rutin-loaded chitosan nanoparticles using agar well diffusion method against *S. aureus* strains (**A**) SA04, (**B**) ATCC 25923, and (**C**) Compared average Inhibition zone diameter (mm) of *S. aureus* strains in various concentrations of Rutin-loaded chitosan nanoparticles by well diffusion assay

Effect of Rut-CS NPs on the Cellular morphology

SEM analysis was conducted to examine the morphological changes induced by Rut-CS NPs in the studied strains when exposed to ½ MIC of the NPs. Figure 11A-C show the normal cell shape and intact cell membrane of untreated SA02, SA04, and ATCC 25923, respectively. After exposure to Rut-CS NPs, the cell morphology underwent significant modifications, and the cell size increased considerably compared to the untreated cells. Figure 11D-F demonstrate that the cell surfaces of the NPs-treated SA02, SA04, and ATCC 25923, respectively were damaged, and evident signs of perturbation such as invagination, rupture lines, and rill-like folds were observed.

Cytoplasm leakage

To investigate the potential effect of Rut-CS NPs on the *S. aureus* cell membrane, the release of DNA was calculated. As demonstrated in Fig. 12, there was a significant difference in DNA concentration among the control and treated groups, implying that the inhibitory effect of Rut-CS NPs on *S. aureus* might be due to cell membrane

Table 1 Average inhibition zone of rutin-loaded chitosan nanoparticles against *S. aureus* strains

Bacteria	Concentration (mg/mL)	Inhibition zone (mm)
ATCC 25923	30	9.33 ± 1.60
	20	9 ± 0.5
	10	6.66 ± 0.7
SA01	30	10.66 ± 0.5
	20	9.33 ± 0.5
	10	7.83 ± 0.2
SA02	30	10.5 ± 0.5
	20	9.33 ± 0.2
	10	8.33 ± 0.2
SA03	30	11.33 ± 0.5
	20	9.5 ± 1.32
	10	7.66 ± 0.7
SA04	30	12.33 ± 0.7
	20	10.06 ± 0.7
	10	7.66 ± 0.5
SA05	30	11.83 ± 0.2
	20	10 ± 0.5
	10	7.83 ± 0.5

damage. To investigate the potential effect of Rut-CS NPs on the *S. aureus* cell membrane, the release of DNA was calculated. As demonstrated in Fig. 12, there was a significant difference in DNA concentration among the control and treated groups, implying that the inhibitory effect of Rut-CS NPs on *S. aureus* might be due to cell membrane damage. In SA01-SA05 strains, DNA leakage at a concentration of ¼ MIC increased by 121.08%, 117.41%, 107.07%, 112.63%, and 109.78%, respectively, compared to the control group. Furthermore, in SA01-SA05 strains, the release of DNA at a concentration of ½ MIC rose by 191.08%, 179.77%, 156.06%, 159.47%, and 157.09%, respectively, in comparison to the control group. Additionally, DNA leakage increased by 112.27% at ¼ MIC and 164.38% at ½ MIC in the ATCC strain compared to the control group.

Hemolysis assay

The impact of sub-minimal inhibitory concentrations (sub-MICs) of Rut-CS NPs on the hemolysin activity of *S. aureus* strains was investigated. The hemolytic activity of the ATCC strain was decreased by 73.55% and 82.59% at ¼ MIC and ½ MIC of Rut-CS NPs, respectively, compared to the control. Also, treating SA01-SA05 with ¼ MIC of Rut-CS NPs reduced hemolysis activity by 57.75%, 58.5%, 54%, 64.75%, and 59.5%, respectively, compared with the control group. Moreover, exposure of SA01-SA05 to ½ MIC of Rut-CS NPs resulted in a reduction in hemolysis activity by 77.5%, 74.5%, 69%, 77%, and 72.5%, respectively, in comparison to the control group (Fig. 13).

Discussion

S. aureus stands as a predominant pathogen responsible for skin and soft tissue infections that carry substantial morbidity and mortality rates. The increasing prevalence of antibiotic-resistant *S. aureus* including

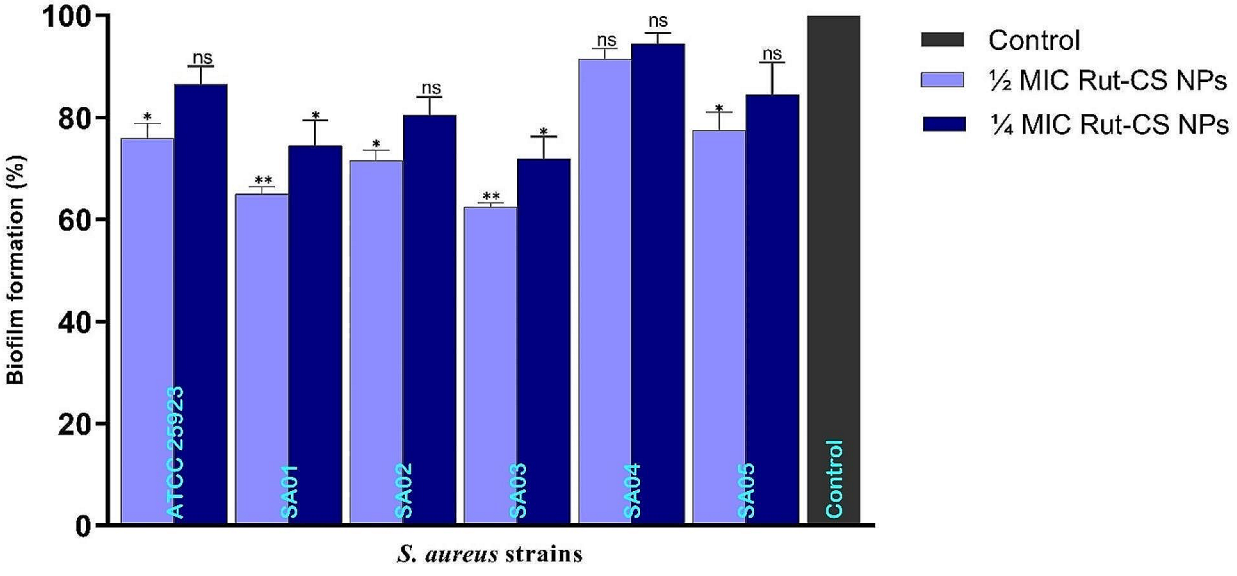

Fig. 8 The effect of the Rutin-loaded chitosan nanoparticles on the biofilm formation by different *S. aureus* strains. Bars indicated the standard deviation of the mean. ** $p < 0.01$, and * $p < 0.05$ indicate statistical significance, whereas ns is non-significance

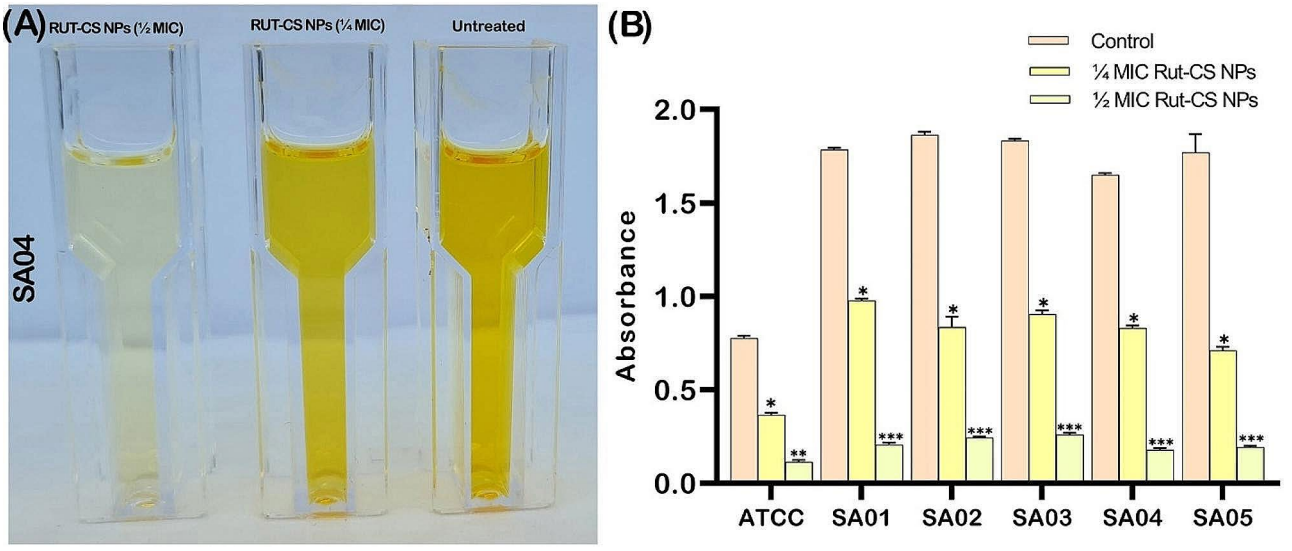

Fig. 9 Inhibitory effect of Rutin-loaded chitosan nanoparticles on the staphyloxanthin production of *S. aureus* strains. (**A**) Qualitative image of staphyloxanthin production, and (**B**) Absorbance value. Bars indicated the standard deviation of the mean. *** $p < 0.0001$, ** $p < 0.01$, and * $p < 0.05$ indicate statistical significance

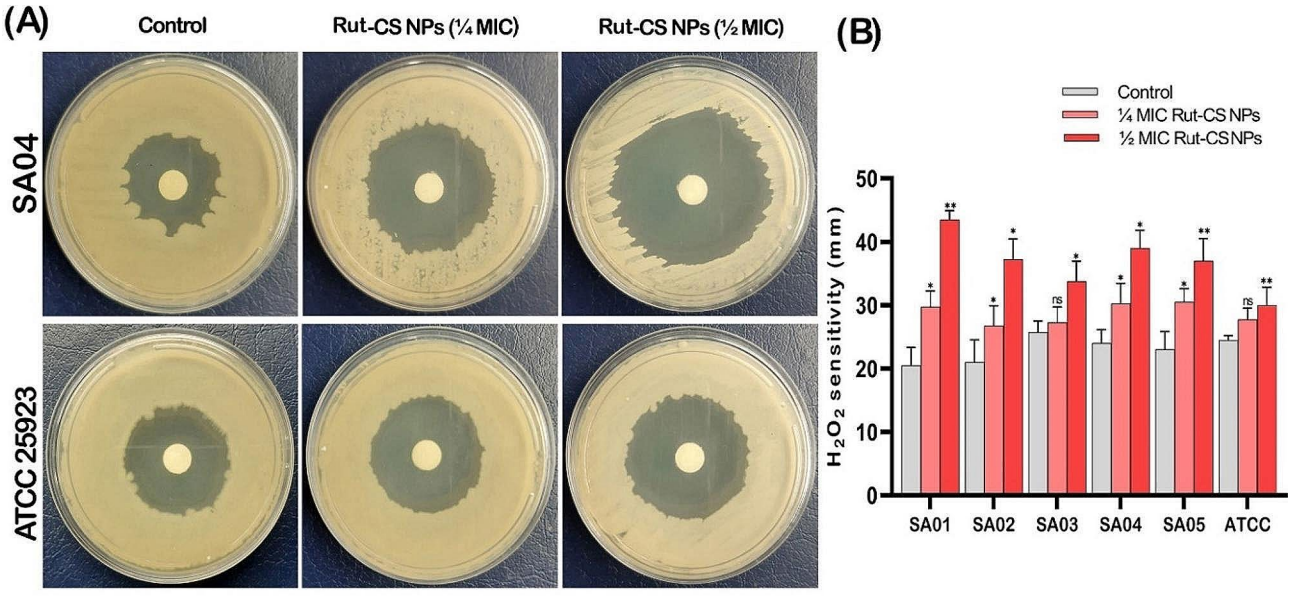

Fig. 10 Hydrogen peroxide sensitivity induced by Rutin-loaded chitosan nanoparticles in *S. aureus* strains. (**A**) Clear halo corresponding to growth inhibition zones of bacterial strains around the hydrogen peroxide disks, and (**B**) Measured diameters of the growth inhibition zones of *S. aureus* strains around the hydrogen peroxide disks. Bars indicated the standard deviation of the mean. ** $p < 0.01$, and * $p < 0.05$ indicate statistical significance, whereas ns is non-significance

penicillin-binding protein 2a (PBP2a) producing strains underscores the necessity for innovative therapeutic approaches [24, 25].

The antibacterial effect of various polyphenols, including curcumin and baicalin, has been determined in previous studies [26, 27]. Rut, classified as an herbal substance within the flavonol group, demonstrates antibacterial and antibiofilm properties against a range of pathogenic strains such as *P. aeruginosa*, *S. aureus*, *Acinetobacter baumannii*, and *E. coli* [4]. However, a significant drawback of polyphenols is their restricted water solubility [28]. Encapsulation of drugs within nanocarriers can enhance their solubility, facilitate their transport, and provide gradual drug release [29]. In 2023, Naseriyeh et al. demonstrated that encapsulating glycyrrhizic acid (GA) in chitosan reduced the release rate of GA [30].

The application of biocompatible polymers leads to achieving prolonged drug release, reduced toxicity, and

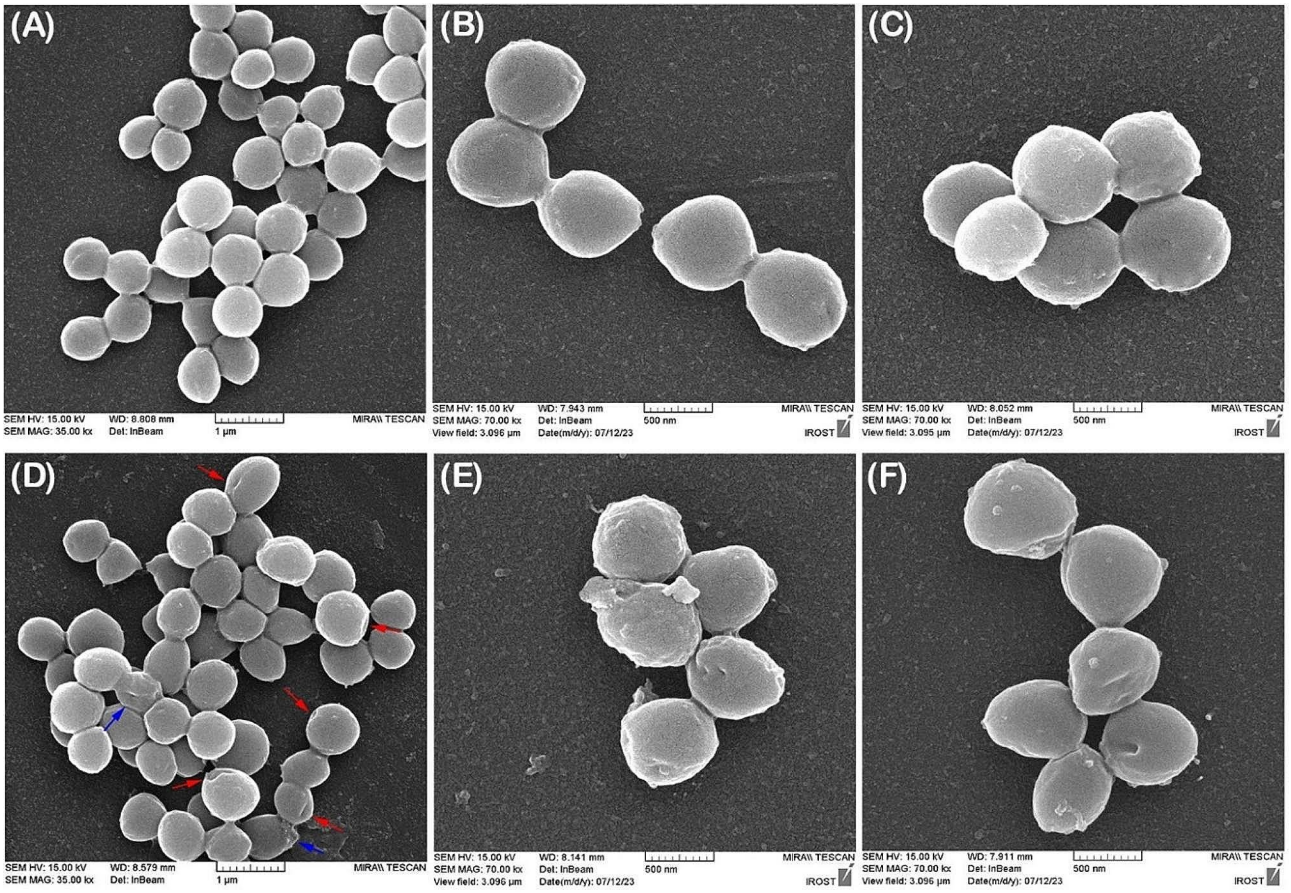

Fig. 11 Scanning electron microscopy analysis of the cells treated with Rutin-loaded chitosan nanoparticles at ½ MIC. The arrow indicates the alteration in cell morphology. (**A**) Untreated SA02; (**B**) Untreated SA04; (**C**) Untreated ATCC 25923; (**D**) Treated SA02; (**E**) Treated SA04; (**F**) Treated ATCC 25923

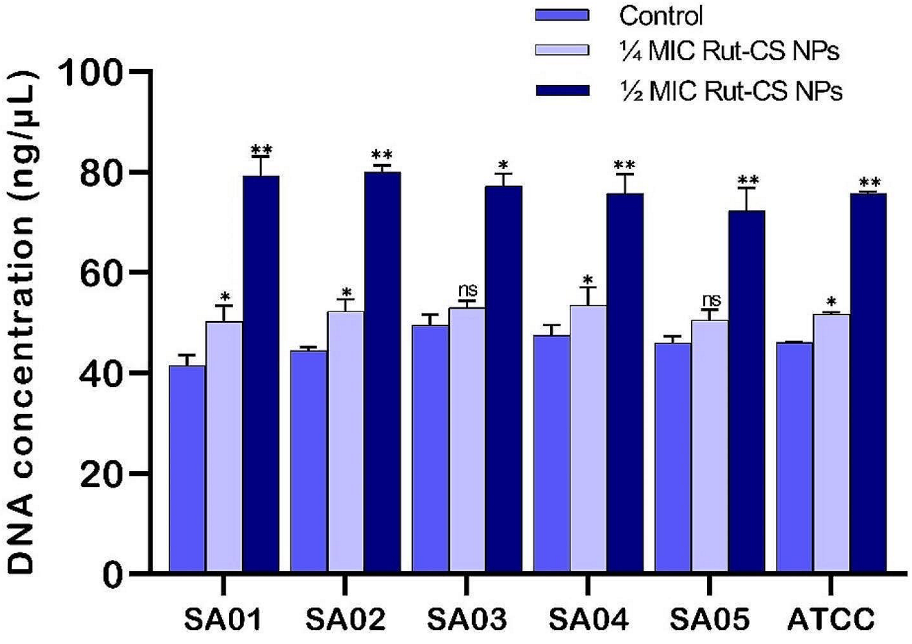

Fig. 12 Leakage of the cytoplasmic nucleic acid of *S. aureus* strains after being treated with ½ and ¼ MIC of Rutin-loaded chitosan nanoparticles. Bars indicated the standard deviation of the mean. ** $p < 0.01$, and * $p < 0.05$ indicate statistical significance, whereas ns is non-significance

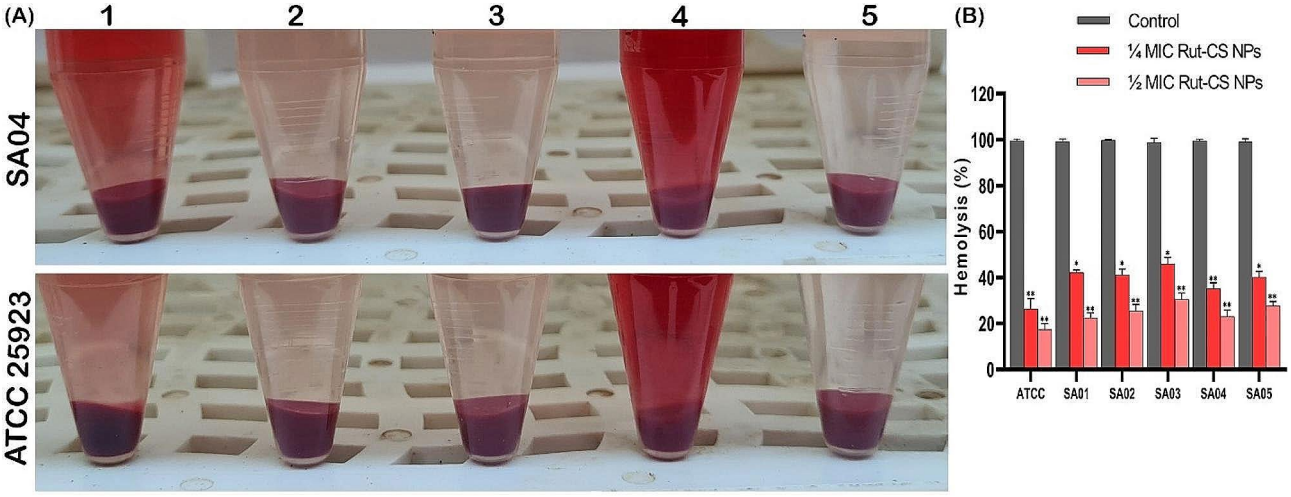

Fig. 13 Effect of ¼ and ½ MIC of Rutin-loaded chitosan nanoparticles on the hemolytic activity of *S. aureus* strains. (**A**) Image of samples after centrifugation at 3000 rpm for 5 min, and (**B**) hemolytic activity (%). (1. Untreated, 2. Treated by ¼ MIC of Rutin-loaded chitosan nanoparticles, 3. Treated by ½ MIC of Rutin-loaded chitosan nanoparticles, 4. Positive control, 5. Negative control). Bars indicated the standard deviation of the mean. ** $p < 0.01$, and * $p < 0.05$ indicate statistical significance

enhanced efficacy of antibacterial agents. They augment drug effectiveness and shield the drug from enzymatic degradation, thus prolonging its activity [31]. CS has gained extensive attention as a nano-carrier due to its non-toxic, biocompatible, and mucoadhesive properties. Furthermore, the antimicrobial and anti-biofilm activities of CS and its nano-derivatives have been documented against a range of microorganisms, including *E. coli*, *Bacillus cereus*, and most other common bacteria [32].

In this study, we encapsulated Rut within CS nanoparticles and examined its impact on clinical strains of *S. aureus* for the first time. The characteristics of the synthesized nanoparticles demonstrated effective entrapment of Rut within the CS matrix. Furthermore, the zeta potential measurement of Rut-CS NPs recorded 37.3 mV, indicating considerable colloidal stability of the nanoparticles.

The agar well diffusion assay was utilized to evaluate the inhibition of bacterial growth. Based on the findings, Rut-CS NPs displayed stronger inhibitory effects compared to CS and Rut alone. This suggests that encapsulation in CS nanoparticles enhances Rut's ability to penetrate the bacterial membrane. This enhancement arises from the interaction between the positive charge of CS and the negatively charged bacterial cell membrane. Moreover, CS NPs facilitate the sustained release of Rut, thereby enhancing its antibacterial efficacy [33].

Biofilms are structured bacterial communities enclosed in a self-produced polymer matrix. They facilitate bacterial escape from the host's immune system and lead to resistance to common antibiotics [34]. The crystal violet staining assay showed a noteworthy reduction in biofilm formation among *S. aureus* strains upon treatment with Rut-CS NPs. Consistent with our findings, prior research has shown that Rut substantially diminishes biofilm formation by *S. aureus* [35]. The anti-biofilm potential of Rut-CS NPs is likely due to chitosan's positive charge, which enables it to interact with negatively charged biofilm components such as extracellular DNA (eDNA). This interaction results in cell membrane damage and leakage of cellular contents, subsequently hindering the biofilm formation process [36]. Furthermore, Rut induces membrane damage, leading to the release of intracellular components, ultimately disrupting the formation of bacterial biofilms [37]. Biofilm formation protects *S. aureus* from host defenses and facilitates infection expansion. Consequently, the inhibition of biofilm formation by Rut-CS NPs plays a crucial role in reducing the pathogenicity of *S. aureus*.

In this investigation, the utilization of NPs remarkably diminished the level of staphyloxanthin pigments in *S. aureus* strains. Since staphyloxanthin possesses antioxidant properties, suppressing this pigment will lower the resistance of *S. aureus* to reactive oxygen species (ROS) [38]. In the H_2O_2 sensitivity assay, it was observed that *S. aureus* strains treated with Rut-CS NPs exhibited heightened sensitivity to oxidative stress compared to the control group. This may be a result of rutin's irreversible alteration of the bacterial membrane, causing pore formation and leakage of intracellular components. Furthermore, the reduction in staphyloxanthin levels correlates with an enhanced susceptibility to H_2O_2.

SEM imaging was conducted to confirm the impact of Rut-CS NPs on bacterial cell morphology. Based on the results, NPs caused significant changes in the bacterial cells, including membrane damage, pore formation, and cell lysis. These findings demonstrate rutin's ability to damage the cell wall. Additionally, electrostatic

interactions between positively charged CS (due to the amino groups of glucosamine) and negatively charged cell membranes (due to the phosphate groups) cause irreversible changes in the cell wall [33].

We also examined the effect of NPs on the leakage of DNA. Our results revealed a significant increase in nucleic acid concentration following NPs treatment compared to the control group. Similar to our findings, a previous study showed that natural products lead to an increased release of nucleic acids and proteins from *S. aureus* [39]. The leakage of cytoplasmic contents after Rut treatment is related to membrane damage and increased cell permeability, as affirmed by the examination of cell morphology in our study.

Targeting the host cell membrane is one critical facet of *S. aureus* virulence. *S. aureus* secretes β-hemolysin, acting as a phospholipase C (PLC), albeit incapable of forming pores in the cell membrane. PLC is a specific neutral sphingomyelinase that hydrolyzes sphingomyelin (a plasma membrane lipid) into ceramide and choline phosphate, contributing to target cell membrane damage [40]. In the present study, sub-MICs of Rut-CS NPs significantly reduced hemolytic activity in the studied strains. Hemolysins assist in lysing the host cell membrane, impairing or evading the immune system, and disease progression. Therefore, the reduction in hemolysin production by different strains of *S. aureus* after treatment with Rut-CS NPs highlights the antibacterial potential of the synthesized nanoparticles.

In summary, the antibacterial mechanisms of Rut-CS NPs against *S. aureus* involve a synergy between the intrinsic antibacterial properties of CS, the antibacterial activity of Rut, and the delivery and sustained release characteristics of the CS NPs.

Conclusions

In this work, rutin was successfully encapsulated into chitosan nanoparticles using the ionic gelation method. Rutin encapsulation into CS NPs was verified through FTIR, XRD, and TEM analyses. The Rut-CS NPs displayed an amorphous shape with a diameter ranging from 160 to 240 nm. The synthesized NPs exhibited an antibacterial effect against *S. aureus* strains. Following treatment with sub-MICs of Rut-CS NPs, the levels of staphyloxanthin and hemolysin production in *S. aureus* were considerably reduced. Additionally, treatment of *S. aureus* with sub-MIC of Rut-CS NPs resulted in alterations in bacterial morphology, including membrane rupture, cell lysis, and subsequently leakage of cytoplasmic DNA. Moreover, Rut-CS NPs demonstrated inhibitory effects on the biofilm formation of *S. aureus*. In conclusion, Rut-CS NPs have shown significant potential in reducing *S. aureus* virulence factors. Nevertheless, further investigations, including in vivo studies and the utilization of eukaryotic model organisms, are imperative to assess the efficacy of Rut-CS NPs and their potential toxicity.

Acknowledgements
The authors sincerely appreciate Dr. Zamani from the University of Guilan for his knowledge and support throughout this project.

Author contributions
F.E. Contributed to the conceptualization, Performed the experiments, Performed the statistical analyses, Wrote the original manuscript draft, and Prepared figures. H.Z. Study design, Project administration, Supervision, Technical support, Data curation, Writing, Review & editing, Resources. All authors read and approved the final manuscript.

Funding
This research did not receive any specific grant from funding agencies in the public, commercial, or not-for-profit sectors.

Data availability
The majority of the data used to support the findings of this study were included in the manuscript. In addition, the additional data are available from the corresponding author upon reasonable request.

Declarations

Ethics approval and consent to participate
Not applicable.

Consent for publication
Not applicable.

Competing interests
The authors declare no competing interests.

Received: 9 October 2023 / Accepted: 26 July 2024
Published online: 07 September 2024

References

1. Turner NA, Sharma-Kuinkel BK, Maskarinec SA, Eichenberger EM, Shah PP, Carugati M, et al. Methicillin- resistant *Staphylococcus aureus*: an overview of basic and clinical research. Nat Rev Microbiol. 2019. https://doi.org/10.1038/s41579-018-0147-4.
2. Abdulbaqi A, Ibrahim AS. Molecular analysis of *Staphylococcus aureus* isolated from clinical samples and natural flora. Cell Mol Biol. 2023. https://doi.org/10.14715/cmb/2022.69.1.25.
3. Yao J, Zou P, Cui Y, Quan L, Gao C, Li Z, et al. Recent advances in strategies to Combat Bacterial Drug Resistance: Antimicrobial materials and Drug Delivery systems. Pharmaceutics. 2023. https://doi.org/10.3390/pharmaceutics15041188.
4. Dehelean CA, Marcovici I, Soica C, Mioc M, Coricovac D, Iurciuc S, et al. Plant-Derived Anticancer compounds as New perspectives in Drug Discovery and Alternative Therapy. Molecules. 2021. https://doi.org/10.3390/molecules26041109.
5. Negahdari R, Bohlouli S, Sharifi S, Maleki Dizaj S, Rahbar Saadat Y, Khezri K, et al. Therapeutic benefits of rutin and its nanoformulations. Phytother Res. 2020. https://doi.org/10.1002/ptr.6904.
6. Sharma S, Ali A, Ali J, Sahni JK, Baboota S. Rutin: therapeutic potential and recent advances in drug delivery. Expert Opin Investig Drugs. 2013. https://doi.org/10.1517/13543784.2013.805744.
7. Kahrizi D, Mohammadi S. Anticancer, antimicrobial, cardioprotective, and neuroprotective activities of luteolin: a systematic-narrative mini-review. Nano Micro Biosyst. 2023. https://doi.org/10.22034/nmbj.2023.403963.1022.
8. Javid H, Ahmadi S, Mohamadian E. Therapeutic applications of apigenin and its derivatives: micro and nano aspects. Micro Nano Bio Aspects. 2023. https://doi.org/10.22034/MNBA.2023.388488.1025.
9. Rivera Aguayo P, Bruna Larenas T, Alarcón Godoy C, Cayupe Rivas B, González-Casanova J, Rojas-Gómez D, et al. Antimicrobial and Antibiofilm Capacity of

Chitosan nanoparticles against Wild Type strain of *Pseudomonas* sp. Isolated from milk of cows diagnosed with bovine mastitis. Antibiotics. 2020. https://doi.org/10.3390/antibiotics9090551.
10. Liao C, Wang Z, Li H, Zhao F, Ling L. Effect of Chitosan-assisted combination of laparoscope and hysteroscope on the levels of IFN-γ and ICAM-1 in treatment of infertility caused by obstruction of fallopian tubes: levels of IFN-γ and ICAM-1 in treatment of infertility. Cell Mol Biol. 2023. https://doi.org/10.14715/cmb/2023.69.4.15.
11. Barbosa M, Vale N, Costa FMTA, Martins MCL, Gomes P. Tethering antimicrobial peptides onto chitosan: optimization of azide-alkyne click reaction conditions. Carbohydr Polym. 2017. https://doi.org/10.1016/j.carbpol.2017.02.050.
12. Deka C, Aidew L, Devi N, Buragohain AK, Kakati DK. Synthesis of curcumin-loaded chitosan phosphate nanoparticle and study of its cytotoxicity and antimicrobial activity. J Biomater Sci Polym Ed. 2016. https://doi.org/10.1080/09205063.2016.1226051.
13. Siddhardha B, Pandey U, Kaviyarasu K, Pala R, Syed A, Bahkali AH, et al. Chrysin-Loaded Chitosan nanoparticles potentiates Antibiofilm activity against *Staphylococcus aureus*. Pathogens. 2020. https://doi.org/10.3390/pathogens9020115.
14. Tran TT, Hadinoto K. A potential quorum-sensing inhibitor for Bronchiectasis Therapy: quercetin–Chitosan Nanoparticle Complex Exhibiting Superior Inhibition of Biofilm formation and swimming motility of *Pseudomonas aeruginosa* to the native quercetin. Int J Mol Sci. 2021. https://doi.org/10.3390/ijms22041541.
15. Fan W, Yan W, Xu Z, Ni H. Formation mechanism of monodisperse, low molecular weight chitosan nanoparticles by ionic gelation technique. Colloids Surf B Biointerfaces. 2012. https://doi.org/10.1016/j.colsurfb.2011.09.042.
16. Alavi M, Karimi N. Antiplanktonic, antibiofilm, antiswarming motility and antiquorum sensing activities of green synthesized Ag-TiO2, TiO2-Ag, Ag-Cu and Cu-Ag nanocomposites against multi-drug-resistant bacteria. Artif Cells Nanomed Biotechnol. 2018. https://doi.org/10.1080/21691401.2018.1496923.
17. Zahmatkesh H, Mirpour M, Zamani H, Rasti B, Rahmani FA, Padasht N. Effect of samarium oxide nanoparticles on virulence factors and motility of multidrug resistant *Pseudomonas aeruginosa*. World J Microbiol Biotechnol. 2022. https://doi.org/10.1007/s11274-022-03384-4.
18. Das S, Dash HR. Microbial biotechnology—a laboratory manual for bacterial systems. New Delhi: Springer; 2014.
19. Kossakowska-Zwierucho M, et al. Factors determining Staphylococcus aureus susceptibility to photoantimicrobial chemotherapy: RsbU activity, staphyloxanthin level, and membrane fluidity. Front Microbiol. 2016. https://doi.org/10.3389/fmicb.2016.01141.
20. Yang Y, Kitajima M, Pham TP, Yu L, Ling R, Gin KY, et al. Using Pseudomonas aeruginosa PAO1 to evaluate hydrogen peroxide as a biofouling control agent in membrane treatment systems. Lett Appl Microbiol. 2016. https://doi.org/10.1111/lam.12674.
21. Côté H, Pichette A, Simard F, et al. Balsacone C. a New Antibiotic Targeting Bacterial cell membranes, inhibits clinical isolates of Methicillin-Resistant *Staphylococcus aureus* (MRSA) without inducing resistance. Front Microbiol. 2019. https://doi.org/10.3389/fmicb.2019.02341.
22. Virto R, Mañas P, Alvarez I, Condon S, Raso J. Membrane damage and microbial inactivation by chlorine in the absence and presence of a chlorine-demanding substrate. Appl Environ Microbiol. 2005. https://doi.org/10.1128/AEM.71.9.5022-5028.2005.
23. Esnaashari F, Rostamnejad D, Zahmatkesh H, Zamani H. In vitro and in silico assessment of anti-quorum sensing activity of Naproxen against *Pseudomonas aeruginosa*. World J Microbiol Biotechnol. 2023. https://doi.org/10.1007/s11274-023-03690-5.
24. Tong SYC, Davis JS, Eichenberger E, Holland TL, Fowler VG. *Staphylococcus aureus* infections: Epidemiology, pathophysiology, clinical manifestations, and management. Clin Microbiol Rev. 2015. https://doi.org/10.1128/CMR.00134-14.
25. Anwer R. Identification of small molecule inhibitors of penicillin-binding protein 2a of methicillin-resistant *Staphylococcus aureus* for the therapeutics of bacterial infection: inhibitors of PBP2a of methicillin-resistant *S. Aureus*. Cell Mol Biol. 2024. https://doi.org/10.14715/cmb/2024.70.3.6.
26. Hussain Y, Alam W, Ullah H, et al. Antimicrobial potential of Curcumin: therapeutic potential and challenges to clinical applications. Antibiot (Basel). 2022. https://doi.org/10.3390/antibiotics11030322.
27. Luo J, Dong B, Wang K, et al. Baicalin inhibits biofilm formation, attenuates the quorum sensing-controlled virulence and enhances *Pseudomonas aeruginosa* clearance in a mouse peritoneal implant infection model. PLoS ONE. 2017. https://doi.org/10.1371/journal.pone.0176883.
28. Kaur H, Kaur GA. Critical Appraisal of solubility enhancement techniques of polyphenols. J Pharm (Cairo). 2014. https://doi.org/10.1155/2014/180845.
29. De R, Mahata MK, Kim KT. Structure-based varieties of polymeric nanocarriers and influences of their Physicochemical properties on Drug Delivery profiles. Adv Sci (Weinh). 2022. https://doi.org/10.1002/advs.202105373.
30. Naseriyeh T, Kahrizi D, Alvandi H, Aghaz F, Nowroozi G, Shamsi A, Hosseini O, Arkan E. Glycyrrhizic acid delivery system Chitosan-coated liposome as an adhesive anti-inflammation. Cell Mol Biol. 2023. https://doi.org/10.14715/cmb/2023.69.4.1.
31. Dorati R, DeTrizio A, Spalla M, Migliavacca R, Pagani L, Pisani S, et al. Gentamicin sulfate PEG-PLGA/PLGA-H nanoparticles: screening design and antimicrobial effect evaluation toward clinic bacterial isolates. Nanomaterials. 2018. https://doi.org/10.3390/nano8010037.
32. Chandrasekaran M, Kim KD, Chun SC. Antibacterial activity of Chitosan nanoparticles: a review. Processes. 2020. 0.3390/pr8091173.
33. Tsai GJ, Su WH. Antibacterial activity of shrimp chitosan against *Escherichia coli*. J Food Prot. 1999. https://doi.org/10.4315/0362-028x-62.3.239.
34. Donlan RM, Costerton JW, Biofilms. Survival mechanisms of clinically relevant Microorganisms. Clin Microbiol Rev. 2002. https://doi.org/10.1128/CMR.15.2.167-193.2002.
35. Al-Shabib N, Abdulatif, et al. Rutin inhibits mono and multi-species biofilm formation by foodborne drug resistant *Escherichia coli* and *Staphylococcus aureus*. Food Control. 2017. https://doi.org/10.1016/j.foodcont.2017.03.004.
36. Wang N, Ji Y, Zhu Y, Wu X, Mei L, Zhang H, et al. Antibacterial effect of chitosan and its derivative on *Enterococcus faecalis* associated with endodontic infection. Exp Ther Med. 2020. https://doi.org/10.3892/etm.2020.8656.
37. Xia X, Song X, Li Y, et al. Antibacterial and anti-inflammatory ZIF-8@Rutin nanocomposite as an efficient agent for accelerating infected wound healing. Front Bioeng Biotechnol. 2022. https://doi.org/10.3389/fbioe.2022.1026743.
38. Clauditz A, Resch A, Wieland KP, Peschel A, Götz F. Staphyloxanthin plays a role in the fitness of *Staphylococcus aureus* and its ability to cope with oxidative stress. Infect Immun. 2006. https://doi.org/10.1128/IAI.00204-06.
39. Chen H, Xu Y, Chen H, Liu H, Yu Q, Han L. Isolation and identification of Polyphenols from Fresh Sweet Sorghum stems and their antibacterial mechanism against foodborne pathogens. Front Bioeng Biotechnol. 2022. https://doi.org/10.3389/fbioe.2021.770726.
40. Guan Z, Liu Y, Liu C, Wang H, Feng J, Yang G. *Staphylococcus aureus* β-Hemolysin Up-Regulates the expression of IFN-γ by human $CD56^{bright}$ NK cells. Front Cell Infect Microbiol. 2021. https://doi.org/10.3389/fcimb.2021.658141.

Publisher's Note